

# Thermal, Optical, and Dielectric Properties of Bio-based Polyimides Derived from an Isosorbide-containing Dianhydride and Diamines with Long Alkyl Chains

Ririka Sawada<sup>1</sup>, Kazuhisa Yajima<sup>2</sup>, Atsuhide Takao<sup>2</sup>,  
Haonan Liu<sup>1</sup>, and Shinji Ando<sup>1\*</sup>

<sup>1</sup> Department of Chemical Science and Engineering, Tokyo Institute of Technology,  
Ookayama, 2-12-1-E4-5, Meguro-ku, Tokyo 152-8552, Japan

<sup>2</sup> Research Center, Honshu Chemical Industry Co., Ltd.,  
Kozaiika 2-5-115, Wakayama-shi, Wakayama 641-0007, Japan

\*ando.s.aa@m.titech.ac.jp

A series of novel semi-aliphatic polyimides (PIs) were synthesized from a dianhydride containing bio-derived isosorbide (ISSDA) moiety and three types of aliphatic diamines with long alkyl chains including a bio-based dimer diamine (DDA). The bio-based content ( $C_B$ ) of the ISSDA-DDA PI is as high as 65 wt%. The PIs derived from ISSDA and aliphatic diamines (ISS-APIs) exhibit excellent optical properties, such as very low refractive indices ( $n_{av} < 1.566$ ) and birefringence ( $\Delta n < 0.00124$ ). These are attributable to the flexible alkyl chains in the PIs which reduce the intermolecular interactions and the orientation of main chains. Furthermore, the low polarity of alkyl chains and the low content of polar groups in the PIs also decrease the electronic polarizability and local oscillating motions, resulting in excellent dielectric properties, such as very low dielectric constants ( $D_k < 2.938$ ) and dissipation factors ( $D_f < 0.00964$ ) at high frequencies (10 and 20 GHz). Despite their low glass transition temperatures of 47–152°C, the 5 wt% weight-loss temperatures of ISS-APIs are as high as 400 °C. This study demonstrates the characteristic properties of the semi-aliphatic PIs which exhibit excellent optical, dielectric, and thermal properties while maintaining high  $C_B$ .

**Keywords:** Semi-aliphatic polyimides, Isosorbide, Alkyl chains, Refractive index, Birefringence, Dielectric constant, Dissipation factor.

## 1. Introduction

In recent years, the use of biomass-based chemical resources has attracted considerable attention from the viewpoint of reducing the environmental load and enhancing sustainability. Bio-based polymers using renewable resources have been widely applied to conventional polymers such as polycarbonate (PC), polyester, polyamide (PA), and epoxy resins [1–6]. The incorporation of bio-based components into the main chains of polymers is expected to reduce the burden on the environment and encourage a sustainable nature. Isosorbide (ISS), a type of 1,4;3,6-dianhydrohexitols (isohexides), is a diol with a bulky and rigid alicyclic structure that is produced from renewable biomass resources such as cellulose (Fig. 1) [2,7]. Its unique structure, low cost, and

available mass production have led to extensive research on its application to engineering plastics such as PCs and polyesters, as well as conventional polymers [1,2,8–10].

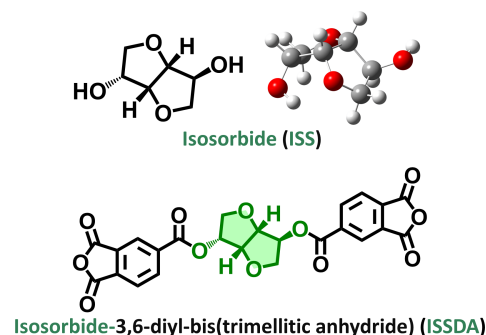


Fig. 1. Chemical structures of isosorbide (ISS) and isosorbide-derived dianhydride (ISSDA).

Polyimides (PIs) are excellent super-engineered polymers with extremely high thermal resistance, chemical stability, electrical insulation, and mechanical strength. Because of their excellent physical properties, PIs play an important role in the microelectronics and aerospace industries. For instance, they have been applied to flexible printed circuit boards, interlayer dielectrics with thermal insulation, and solar sails [11]. In addition, PIs are expected to be useful in optical, electronic, and dielectric applications, such as optical waveguides, light-wave components, organic light-emitting devices (OLEDs), substrates for flexible OLED displays, dielectrics for high-frequency wireless communication, and organic solar cells in recent years [12–15]. For these applications, PIs should exhibit high optical transparency, low refractive index, small birefringence, low dielectric constant ( $D_k$ ), and dissipation factor ( $D_f$ ), as well as sufficient heat resistance and mechanical strength. Wholly aromatic or semi-aliphatic PIs are the best candidates for achieving these requirements. However, conventional aromatic PIs have critical problems, such as strong coloration caused by the inter- and intramolecular charge-transfer (CT) interactions [16–19], high  $D_k$  due to the polar imide groups, and poor processability owing to the rigid backbones [20–22]. For example, the earliest and the most conventional PI derived from pyromellitic dianhydride (PMDA) and 4,4'-diaminodiphenyl ether (4,4'-ODA) (PMDA-ODA, Kapton by DuPont) has a dark yellow color and a high dielectric constant ( $D_k = 3.44$  at 10 GHz). These are due to the high planarity of the repeating unit and the strong intra- and intermolecular CT interactions between the aromatic moieties [23]. Besides, most of the wholly aromatic PIs do not possess melt processability and solubility due to their rigid main chain and high glass transition temperatures ( $T_g$ ).

To overcome these shortcomings, PIs exhibiting high optical transparency, low refractive indices, small birefringence, and low water absorption as well as low  $D_k$  and  $D_f$  are in strong demand. For example, aliphatic PIs are preferable because the bulky, non-coplanar, and low-polarizable aliphatic moieties inhibit CT interactions and suppress intermolecular packing. Wholly aliphatic PIs exhibit high optical transparency in the UV and visible regions, and low refractive indices and  $D_k$  which cannot be achieved by wholly and semi-aromatic PIs [24,25]. Aliphatic PIs, composed of linear alkyl chains in the main structures, are also superior to aromatic ones in terms of melt processability owing

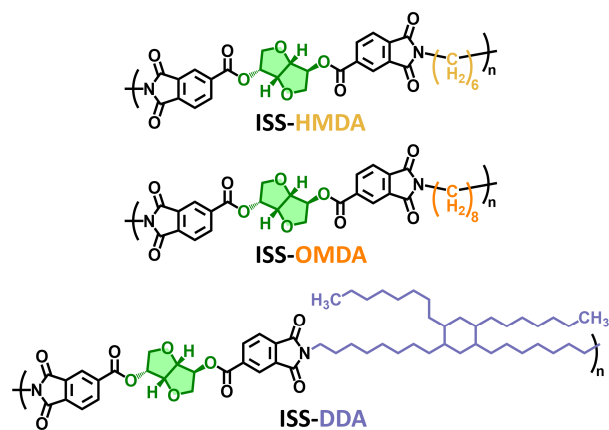


Fig. 2. Chemical structures of three types of ISS-APIs.

to the flexibility of methylene ( $\text{CH}_2$ ) units as well as excellent optical and dielectric properties [21,22]. Recently, dimer diamines, a type of wholly aliphatic bio-based diamines composed of long and branched alkyl chains, have attracted attention because bio-based content ( $C_B$ ) of more than 50 % can be achieved by introducing it into PIs. However, the PI films containing long alkyl moieties frequently become brittle due to the semi-crystallinity of the alkyl chains, and the thermal stability deteriorates as represented by low  $T_g$ s ( $< 100$  °C) [20,26,27]. For instance, the PIs synthesized from a dimer diamine and conventional aromatic dianhydrides exhibit  $T_g$ s close to or lower than room temperature, despite their improved thermoplastic processability [28–31].

We have previously reported a series of novel semi-aliphatic PIs (ISS-PIs) synthesized from a bio-based dianhydride derived from isosorbide (ISSDA) (Fig. 1), which exhibit excellent optical transparency, low refractive indices, and low  $D_k$  at high frequencies of 10 and 20 GHz, with sufficient thermal stability [32,33]. By combining ISSDA which contains a bulky aliphatic ISS moiety with long alkyl diamines or dimer diamines that have low polarity and flexibility, the new PIs are expected to exhibit better optical and dielectric properties while maintaining high  $C_B$  and thermal resistance.

In this study, three types of semi-aliphatic PIs incorporating long alkyl chains by 1,6-hexamethylene diamine (HMDA), 1,8-octamethylene diamine (OMDA), or dimer diamine (DDA) and a bio-based ISS moiety in the main chain, namely ISS-APIs, were synthesized. (Fig. 2). Their optical and dielectric properties, such as optical transparency, refractive indices and birefringence,  $D_k$  and  $D_f$  at high frequencies (10 and 20 GHz) were investigated in addition to the thermal and mechanical properties. The structure-property relationship of the ISS-APIs was also discussed

based on their structural flexibility, polarity, and intermolecular interactions.

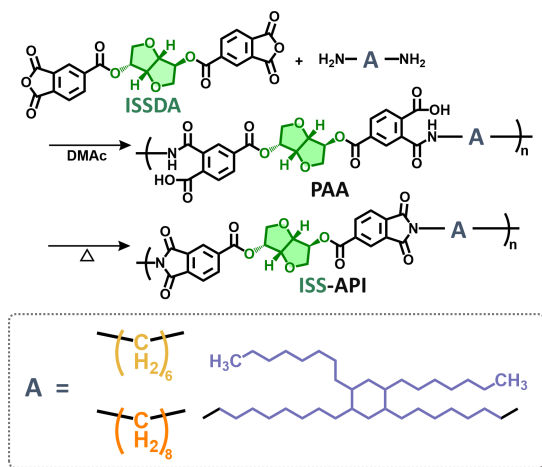
## 2. Experimental

### 2.1. Materials

Isosorbide was purchased from Sigma-Aldrich Co. LLC (Missouri, USA). Trimellitic anhydride chloride, 1,6-hexamethylenediamine (HMDA), and 1,8-octamethylenediamine (OMDA) were purchased from Tokyo Chemical Industry (TCI, Tokyo, Japan) Co., Ltd. A dimer diamine (Priamine 1075, DDA) was generously offered from Cargill Bioindustrial B.V. *N,N*-Dimethylacetamide (DMAc), *N*-methyl-2-pyrrolidone (NMP),  $\gamma$ -butyrolactone (GBL), cyclohexanone (CHXO), cyclopentanone (CPNO), and dimethyl sulfoxide- $d_6$  (DMSO- $d_6$ ,  $\geq 99.9$  atom%D) were purchased from Fujifilm Wako Pure Chemical Corporation (Osaka, Japan) and used without further purification. Moisture in DMAc was controlled under 0.01wt% by adding molecular sieves, which was confirmed by a Karl Fischer titrator (MKS-520, Kyoto Electronic Manuf. Co., Ltd. (Kyoto, Japan)).

### 2.2. Preparation of ISS-API films

The synthesis of ISSDA dianhydride has been reported elsewhere [32]. Three types of ISS-APIs (Fig. 2) were prepared from ISSDA and aliphatic diamines using a typical two-step method, as shown in Scheme 1. To prepare the corresponding precursors, namely poly(amic acid)s (PAAs), linear diamines (HMDA (0.465 g, 4 mmol) and OMDA (0.577 g, 4 mmol)) were dissolved in DMAc and stirred at 0 °C for 2–3 h, followed by the addition of ISSDA with an equimolar amount of each diamine (1.977 g, 4 mmol) and stirring at room temperature for 48 h. The PAA of ISS-DDA was synthesized



Scheme 1. Two-step synthetic procedure of ISS-APIs via PAA precursors.

under the same condition but with a 10% excess of DDA. The solid contents of the PAA solutions were set to 20 wt%. The PAA solutions thus obtained were cast onto a glass substrate, dried at 70 °C for 50 min, and then thermally cured under  $N_2$  flow at a heating rate of 3 °C/min up to 280 °C. The temperature was kept for 90 min and then cooled to room temperature.

### 2.3. Measurements

#### 2.3.1. Optical analyses

Infrared (IR) absorption spectra were collected using a Fourier-transform infrared (FT-IR) spectrometer (FT/IR-4000, JASCO, Tokyo, Japan) equipped with an attenuated total reflection (ATR) apparatus. The spectral resolution and the number of scans were 4  $cm^{-1}$  and 16, respectively.

The in-plane ( $n_{TE}$ ) and out-of-plane ( $n_{TM}$ ) refractive indices were independently measured by the prism coupling method using a Metricon PC-2010 prism coupler (New Jersey, USA) at wavelengths of  $\lambda = 636, 845, 1310, \text{ and } 1558$  nm. The average refractive index ( $n_{av}$ ) and in-plane/out-of-plane birefringence ( $\Delta n$ ) were estimated using eqs. (1) and (2), respectively [34].

$$n_{av} = \sqrt{\frac{2n_{TE}^2 + n_{TM}^2}{3}} \quad (1)$$

$$\Delta n = n_{TE} - n_{TM} \quad (2)$$

The wavelength dispersions of  $n_{av}$  were fitted using eq. (3) according to the simplified Cauchy's formula:

$$n_{av} = n_{\infty} + \frac{B_n}{\lambda^2} \quad (3)$$

where  $n_{\infty}$  is the estimated value of  $n_{av}$  at infinite wavelength and  $B_n$  is the coefficient of wavelength dispersion of  $n_{av}$ .

The UV-visible (UV-vis) optical absorption spectra of PI films were measured using a JASCO V-760 spectrophotometer (Tokyo, Japan). The incident light was *p*-polarized by a Glan-Taylor prism made of calcite crystals (Sigma Koki, Co., Ltd., Tokyo, Japan), and the incident angle was adjusted to Brewster's angle of  $\sim 58^\circ$  to suppress Fresnel reflection at the film surface.

#### 2.3.2. Analysis of dielectric properties

The experimental dielectric constant, *i.e.*, relative permittivity ( $D_k$ ), and dissipation factor, *i.e.*,

dielectric loss ( $D_f$ ), were measured in the transverse electric ( $TE_{011}$ ) mode at 10 and 20 GHz using cavity resonators (AET, Kanagawa, Japan) connected to a vector network analyzer (VNA) (Anritsu MS46122B, Tokyo, Japan). To avoid the influence of the measurement environment, the resonator was stored in a home-built chamber made of acrylic resin, in which the temperature and relative humidity (RH) were controlled at 23 °C and 30%RH, respectively.  $D_k$  and  $D_f$  were determined by averaging the data from five measurements for a 50 mm × 50 mm film. The thickness of the PI films (average 38.1 μm) was measured using a digimatic indicator (ID-H 0530, Mitutoyo, Kanagawa, Japan).

### 2.3.3. Thermo-mechanical analyses

Differential scanning calorimetry (DSC) measurement was performed by a Shimadzu DSC-60 analyzer (Kyoto, Japan) under  $N_2$  flow. DSC measurements for ISS-HMDA and ISS-OMDA were performed in the following cycle: cooling from 250 °C to 60 °C; holding for 5 min; heating from 60 °C to 250 °C; holding for 5 min. For ISS-DDA, DSC measurement was conducted with the following cycle: cooling from 150 °C to -50 °C; holding for 5 min; heating from -50 °C to 150 °C; holding for 5 min. The heating and cooling rates were set to 10 °C/min and -10 °C/min, respectively. To confirm reproducibility, three cycles of DSC were measured, and the DSC charts of second heating were used for the analysis.

Thermomechanical analysis (TMA) was conducted with a Shimadzu TMA-60 analyzer (Kyoto, Japan) with a fixed load of 0.03 N, at a heating rate of 10 °C/min, under  $N_2$  flow. For ISS-HMDA and ISS-OMDA, the first run was conducted from 25 °C to 80 °C to release residual stress. After the sample was cooled to room temperature, the second run was conducted from 50 °C to 180 °C. ISS-DDA was measured from 15 °C to 100 °C. The  $T_g$  was determined from the inflection points of the TMA curves, and the coefficient of linear thermal expansion in the in-plane direction (CTE) was estimated from the slope of the TMA curves in the 50–120 °C range, according to eq. (4) [35]:

$$CTE = \frac{1}{l(T_0)} \cdot \frac{dl}{dT} \quad (4)$$

where  $T$ ,  $T_0$ , and  $l$  represent the absolute temperature, initial temperature before heating ( $T_0 = 50$  °C), and film length, respectively.

Thermogravimetric analysis (TGA) was

conducted using a Shimadzu TGA-50 analyzer (Kyoto, Japan) at a heating rate of 10 °C/min, under  $N_2$  flow. Residual weight was measured in the range of 30–550 °C. The TGA curves were drawn based on the percentage of residual weight relative to the initial weight of the samples, and thus 5 wt% weight loss temperature ( $T_d^5$ ) was evaluated. Dynamic mechanical analysis (DMA) was conducted using a DMA850 (TA Instruments, Delaware, USA) apparatus at a heating rate of 3 °C/min at sinusoidal load, with a frequency of 0.1 Hz, under  $N_2$  flow.

## 3. Results and discussion

### 3.1. Structural characterization and solubility of ISS-APIs

The completion of thermal imidization of the ISS-APIs was confirmed by the ATR-FT-IR spectra (Fig. 3) based on the appearance of the characteristic absorption bands at 1370  $cm^{-1}$  (stretching of imide C–N bonds), 1713  $cm^{-1}$  (asymmetric stretching of imide C=O bonds), and 1775  $cm^{-1}$  (symmetric stretching of imide C=O bonds), and the absence of the peak around 1660  $cm^{-1}$  (amide –CO–NH– bonds). In addition, the characteristic signals assignable to the symmetric and asymmetric stretching of  $CH_2$  were observed at 2945–2923  $cm^{-1}$  and 2859–2853  $cm^{-1}$ , respectively [36], confirming that the alkyl moieties were successfully introduced into the PI main chains. It is also reasonable that the absorbance assigned to the  $CH_2$  stretching vibration increases and the peaks become sharp with an increase in the alkyl chain

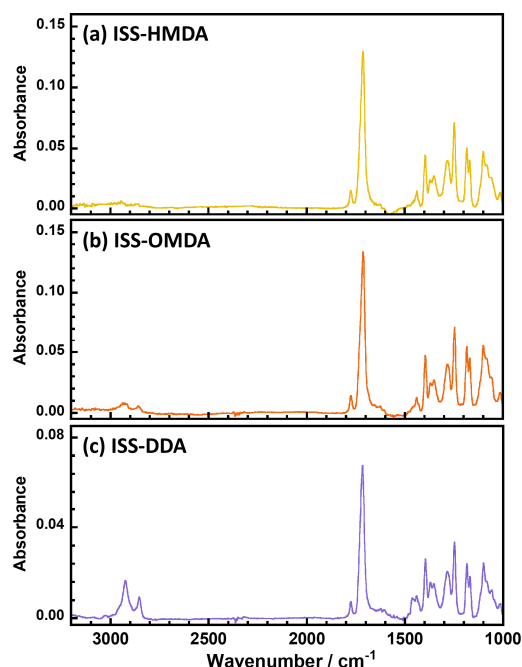


Fig. 3. ATR-FT-IR spectra of ISS-API films.

Table 1. Solubilities of ISS-API films in organic solvents. +: soluble; ±: partially soluble; -: insoluble.

| Polyimide | NMP | DMSO | DMAc | GBL | CHXO | CPNO |
|-----------|-----|------|------|-----|------|------|
| ISS-HMDA  | +   | ±    | +    | +   | ±    | +    |
| ISS-OMDA  | +   | ±    | +    | +   | ±    | +    |
| ISS-DDA   | ±   | ±    | ±    | ±   | ±    | ±    |

length. Note that only ISS-DDA shows a clear peak assignable to the bending of CH<sub>2</sub> at 1463 cm<sup>-1</sup> [36].

Table 1 summarizes the solubility data of the ISS-API films in organic solvents, *i.e.* NMP, DMSO, DMAc, GBL, CHXO, and CPNO. Notably, ISS-APIs are well soluble in low-polar solvents such as GBL and CPNO, as well as polar solvents including NMP and DMSO. The solubility of PIs can be generally enhanced by introducing flexible backbones, bulky non-coplanar moieties, and kinked linkages [26]. The solubility of ISS-APIs in low-polar solvents was improved by the flexible and low-polar long alkyl chains. However, the solubility

of ISS-DDA was slightly poor compared to ISS-HMDA and ISS-OMDA, probably due to the cross-linking structures formed at 280 °C.

### 3.2. Optical properties of ISS-APIs

#### 3.2.1. Refractive indices and birefringence

The wavelength dispersions of  $n_{av}$  and  $\Delta n$  for ISS-APIs are displayed in Fig. 4. The refractive indices ( $n_{TE}$ ,  $n_{TM}$ ,  $n_{av}$ ) and birefringence ( $\Delta n$ ) measured at  $\lambda = 1310$  nm with the fitted parameters of  $n_{\infty}$  and  $B_n$  determined by applying eq. (3) are summarized in Table 2. From Fig. 4 and Table 2, the  $n_{av}$  of ISS-HMDA and ISS-OMDA (1.5657 and 1.5603, respectively) are comparable to those of ISS-DACH and ISS-ADM synthesized from ISSDA and alicyclic *cis*-1,4-cyclohexanediamine or adamantane-1,3-diamine [32], which are significantly lower than aromatic PIs ( $n_{av} \sim 1.652$ ,  $\Delta n \sim 0.076$  [18]). Here, the  $n_{av}$  of a polymer can be described by the Lorentz-Lorenz equation [37]:

$$\frac{n_{av}^2 - 1}{n_{av}^2 + 2} = \frac{N}{3\epsilon_0} \alpha_{av} = \frac{4\pi}{3} \cdot \frac{\rho N_A}{M} \alpha_{av} \quad (5)$$

where  $N$  is the number of repeating units,  $\epsilon_0$  is the vacuum permittivity,  $\alpha_{av}$  is the average polarizability,  $\rho$  is the density of the polymer,  $N_A$  is the Avogadro constant, and  $M$  is the molecular weight of the repeating unit, respectively. Eq. (4) implies that a small polarizability per unit volume ( $\alpha_{av}/V$ ) lowers  $n_{av}$ . Generally, wholly aromatic PIs have a high  $n_{av}$  due to the polar imide groups with a large polarizability and dense packing of the main chains. In contrast, the introduction of alkyl chains which have small polarizabilities and disconnect  $\pi$ -conjugation of the main chain lowers the  $n_{av}$  of PIs based on the eq. (5) [27,32]. The synergistic effect

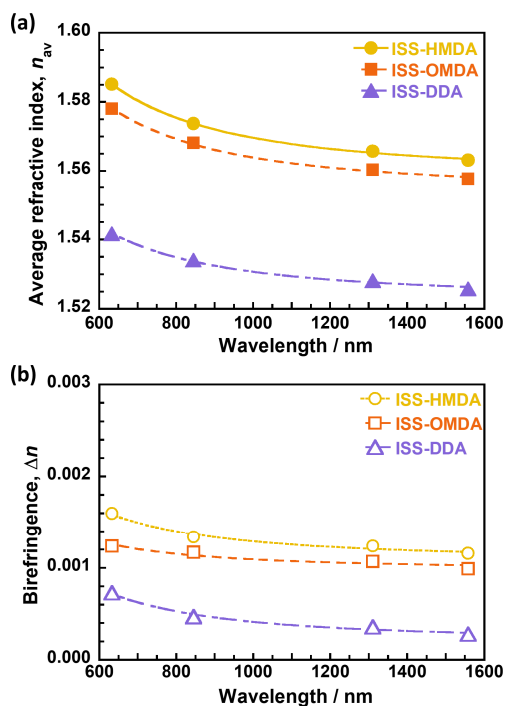


Fig. 4. Wavelength dispersions of (a) average refractive indices ( $n_{av}$ ) and (b) in-plane/out-of-plane birefringence ( $\Delta n$ ) of ISS-APIs.

Table 2. Experimental in-plane, out-of-plane, and average refractive indices ( $n_{TE}$ ,  $n_{TM}$ , and  $n_{av}$ , respectively) and birefringence ( $\Delta n$ ) of ISS-APIs measured at 1310 nm, and the fitted parameters of wavelength dispersion ( $n_{\infty}$ ,  $B_n$ ).

| Polyimide | $n_{TE}$ | $n_{TM}$ | $n_{av}$ | $\Delta n$ | $n_{\infty}$ | $B_n$ |
|-----------|----------|----------|----------|------------|--------------|-------|
| ISS-HMDA  | 1.5661   | 1.5649   | 1.5657   | 0.00124    | 1.5593       | 10373 |
| ISS-OMDA  | 1.5607   | 1.5596   | 1.5603   | 0.00107    | 1.5544       | 9544  |
| ISS-DDA   | 1.5282   | 1.5279   | 1.5281   | 0.00036    | 1.5233       | 7419  |

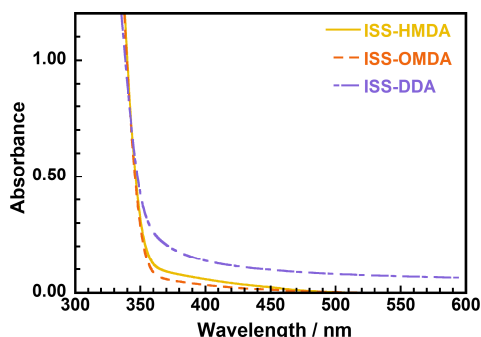


Fig. 5. UV-vis spectra of ISS-API films.

of the inherent bulkiness of ISSDA and the flexibility of alkyl groups can also contribute to the decrease in  $n_{av}$  because it expands interchain free volume and suppresses dense packing. ISS-DDA, which has the largest fraction of aliphatic groups of 25.4 % (= *Alkyl%*; weight sum of alkyl chain and ISS moiety, Table 3), exhibited the lowest  $n_{av}$  (= 1.5281) due to the further reduction of intermolecular interactions by the flexible and long side chains in the DDA unit. This indicates that ISS-DDA is effective in lowering  $n_{av}$  beyond a fluorinated ISS-TFDB derived from ISSDA and 2,2'-bis(trifluoromethyl)-benzidine (TFDB) [32].

Notably, the values of  $\Delta n$  of ISS-APIs are smaller than 0.0016, which is smaller than 1/10 of that of wholly aromatic PIs [18]. The flexible alkyl chains increase the degree of conformational freedom of the main chain, as well as the bulky and bent ISSDA unit, leading to more isotropic chain orientations. ISS-DDA, especially with its long alkyl chains ( $\approx$  C18) and side chains, may have an increased conformational freedom of the main and side chains ( $\approx$  C7–8), resulting in a negligibly small  $\Delta n$ . Furthermore, the coefficient of wavelength dispersion ( $B_n = 7419$ ) and the refractive index at the infinite wavelength ( $n_\infty = 1.5233$ ) are exceptionally small.

### 3.2.2. Optical transparency of ISS-APIs

Fig. 5 shows the UV-vis absorption spectra of ISS-API films normalized by the film thickness. All ISS-APIs exhibit higher optical transparency and

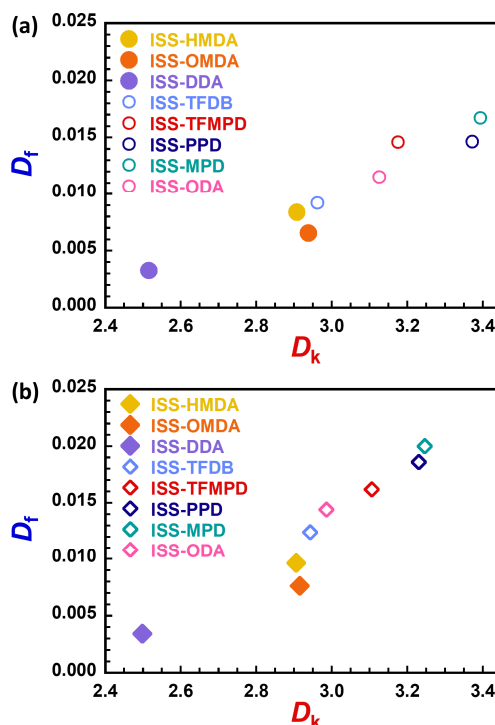


Fig. 6. Dielectric constants ( $D_k$ ) and dissipation factors ( $D_f$ ) of ISS-APIs and those of ISS-PIs [32] measured at (a) 10 GHz and (b) 20 GHz.

suppressed coloration in the visible region, as compared to wholly aromatic PIs, with the cut-off wavelengths of UV absorption below 360 nm. This originates from the reduction of inter- and intramolecular CT interactions due to the alkyl moieties with high flexibility and low polarity [18,26]. Meanwhile, the absorption edge wavelengths of ISS-HMDA and ISS-OMDA are located at 470 nm, suggesting a slight formation of intermolecular CT interactions. The transparency of OMDA is slightly higher than that of HMDA in the 360–470 nm range, which could be due to the suppression of aggregation by CT complex formation by the slightly longer OMDA chains. ISS-DDA is not optically transparent over the entire wavelength range as shown in Fig. 5, presumably due to the light scattering caused by partial micro-phase separation between the fully aliphatic and semi-aromatic domains.

Table 3. Dielectric constants ( $D_k$ ), dissipation factors ( $D_f$ ) measured at 10 and 20 GHz, film thickness ( $d$ ), the weight fraction of aliphatic groups (*Alkyl%*), and that of imide and ester groups per repeating unit (*Polar%*) of ISS-APIs.

| Polyimide | $D_k$  |         | $D_f$  |         | $d / \mu\text{m}$ | <i>Alkyl%</i> / wt% | <i>Polar%</i> / wt% |
|-----------|--------|---------|--------|---------|-------------------|---------------------|---------------------|
|           | 10 GHz | 20 GHz  | 10 GHz | 20 GHz  |                   |                     |                     |
| ISS-HMDA  | 2.908  | 0.00836 | 2.906  | 0.00964 | 37.7              | 18.5                | 32.8                |
| ISS-OMDA  | 2.938  | 0.00653 | 2.915  | 0.00763 | 34.7              | 22.7                | 29.3                |
| ISS-DDA   | 2.516  | 0.00327 | 2.498  | 0.00344 | 41.9              | 25.4                | 23.9                |

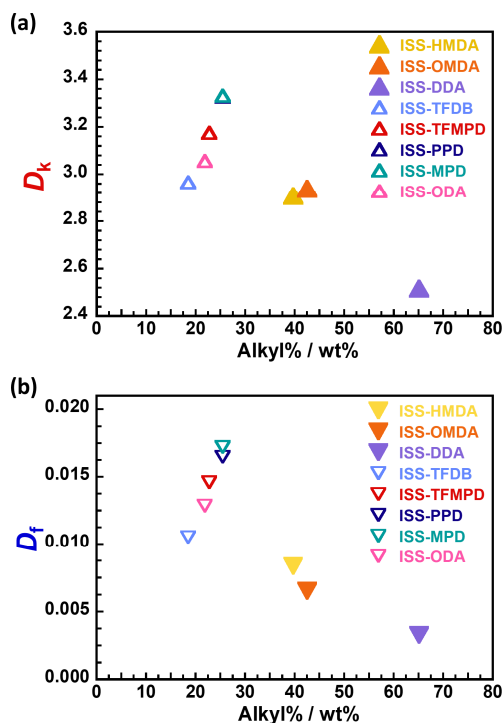


Fig. 7. Relationship between the alkyl group content (*Alkyl%*) and (a)  $D_k$ , (b)  $D_f$  of ISS-APIs and those of ISS-PIs [32] at 10 GHz.

### 3.3. Dielectric properties of ISS-APIs

The experimental dielectric parameters, namely  $D_k$  and  $D_f$ , of ISS-APIs measured at 10 GHz and 20 GHz are shown in Figs. 6 (a) and (b), respectively, and these values are summarized in Table 3. The dielectric data of the ISS-PIs derived from aromatic diamines are also listed as references. ISS-APIs exhibit excellent dielectric properties ( $D_k < 2.938$ ,  $D_f < 0.00964$ ) as novel low-dielectric PIs [38–40]. In particular, ISS-DDA shows significantly small  $D_k$  and  $D_f$  (2.52 and 0.00327 at 10 GHz). The relationship between *Alkyl%* and  $D_k$ ,  $D_f$  shown in Fig. 7 indicates that both  $D_k$  and  $D_f$  decrease with a significant increase in *Alkyl%* for ISS-APIs, even though the  $D_k$  and  $D_f$  of the aromatic ISS-PIs depend on the molecular weight per repeating unit rather than on the *Alkyl%*. Moreover, Fig. 6 shows positive correlations between  $D_k$  and  $D_f$  for a series of ISS-PIs including ISS-APIs at each frequency.

Fig. 8 shows the dependence of  $D_k$  and  $D_f$  of ISS-APIs at 10 GHz on the weight fractions of polar (imide and ester) groups per repeating unit (*Polar%*), respectively. Here, most of the contribution to the  $D_k$  at 10 GHz is attributable to the electronic polarizability ( $\alpha_e$ ) which depends on the chemical structure, indicating that a polar group with a large  $\alpha_e$  increases  $D_k$  [15,41]. For the  $D_k$  in Fig. 8 (a), it is suggested that DDA exhibits the smallest  $D_k$  due to the sufficiently small *Polar%*, *i.e.*,

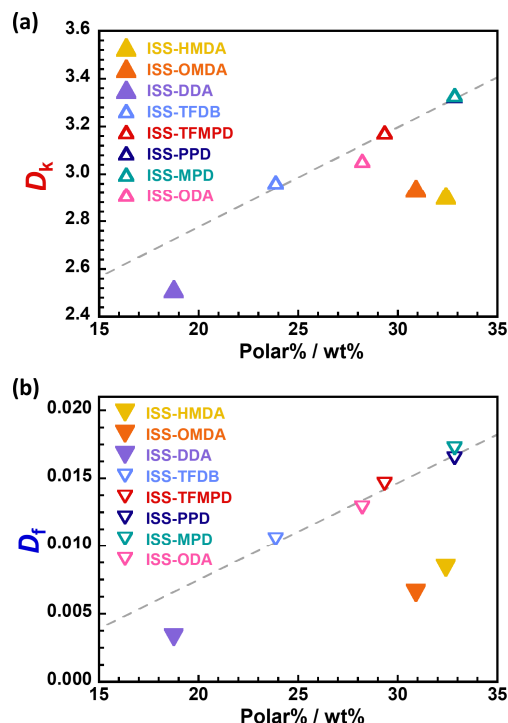


Fig. 8. Relationship between the polar group content (*Polar%*) and (a)  $D_k$ , (b)  $D_f$  of ISS-APIs and ISS-PIs [32] at 10 GHz.

high *Alkyl%*. Furthermore, for all ISS-APIs, their  $D_k$  values deviate below the approximate line derived from the ISS-PIs prepared from aromatic diamines. This is attributable to the smaller  $\alpha_e$  of the long alkyl chains [21,26,32] than that of aromatic groups, resulting in smaller  $D_k$ s of ISS-APIs than those expected from the *Polar%*.

The primary origin of the  $D_f$  at 10 GHz is local oscillating motions of polar groups, rather than electronic polarization. Fig. 8 (b) clearly shows that the  $D_f$  of ISS-DDA is smaller than those of ISS-HMDA and ISS-OMDA, suggesting that the former PI with the smallest *Polar%* has essentially fewer oscillating components under the AC field. In contrast, despite the relatively large *Polar%* and the flexible alkyl chains activating oscillating motions, the  $D_f$  of both ISS-HMDA and ISS-OMDA are smaller than those of the other ISS-PIs. Considering the large deviations of the  $D_f$  of ISS-APIs from the approximate line in Fig. 8 (b), the relaxation time or resonant frequency of the PIs incorporating long alkyl chains could be far different from those of the aromatic main chains. Although it is generally difficult to achieve both a small  $D_k$  and a small  $D_f$  due to the difference in their origins, the incorporation of alkyl chains into the PI main chains is effective in reducing both  $D_k$  and  $D_f$  at a high frequency of 10 GHz.

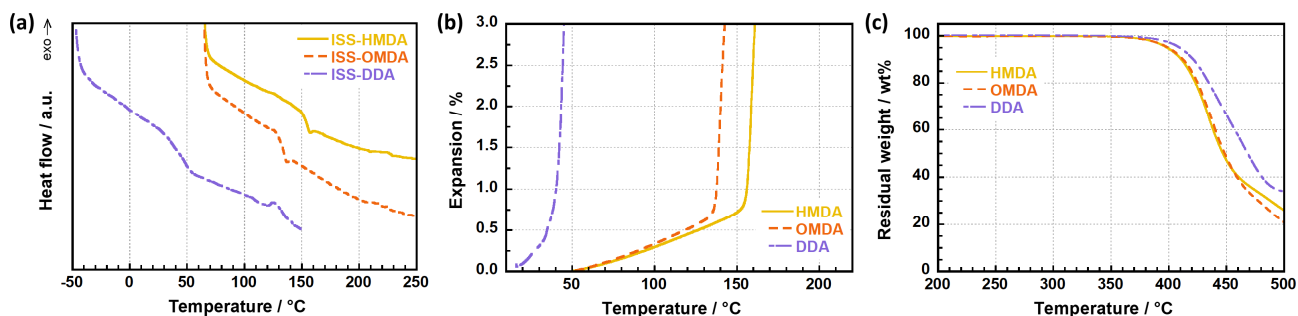


Fig. 9. (a) DSC, (b) TMA, and (c) TGA curves of ISS-APIs.

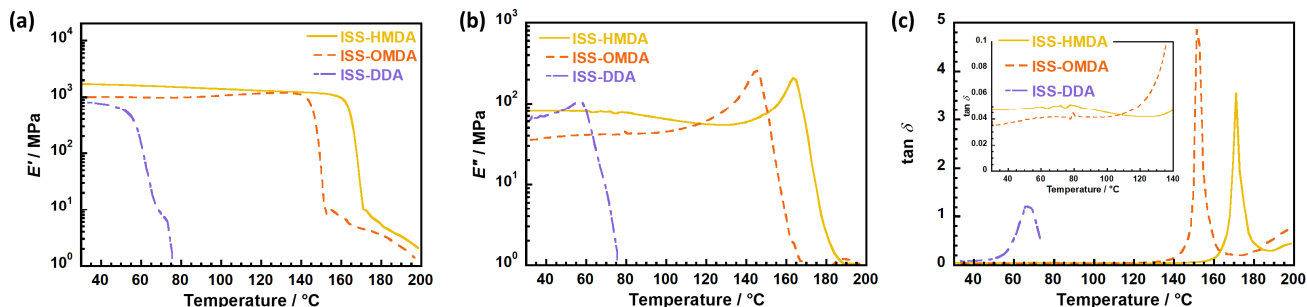


Fig. 10. Temperature dependence of (a) storage modulus ( $E'$ ), (b) loss modulus ( $E''$ ), and (c)  $\tan \delta$  of ISS-APIs.

### 3.4. Thermal properties of ISS-APIs

Fig. 9 shows the DSC, TMA, and TGA curves of ISS-APIs, and the characteristic thermal properties ( $T_g$  from DSC and TMA, CTE, and  $T_d^5$ ) are summarized in Table 4. The comparable  $T_g$  values were obtained from DSC and TMA, and those of ISS-HMDA and ISS-OMDA from TMA curves are 156 °C and 138 °C, respectively, which are lower than those of ISS-PIs by more than 80 °C [32]. In general, aromatic PI exhibit  $T_g$ s higher than 300 °C due to their structural rigidity and strong intermolecular interactions, while the introduction of a linear aliphatic skeleton like alkyl chains significantly increases the flexibility of the main chain [42,43]. Thereby, ISS-DDA which has the longest alkyl chain length and the branched structure exhibited the lowest  $T_g$  below 50 °C. Besides, the ester linkages incorporated in ISSDA are rotatable and increase the degree of conformational freedom, which is an additional

factor in lowering the  $T_g$  compared to wholly aromatic dianhydrides.

From Fig. 9 (c), all the ISS-APIs exhibit  $T_d^5$  values higher than 399 °C, implying that ISS-APIs have sufficient thermal decomposition stability, despite their aliphatic skeleton with weaker covalent bonds. These  $T_d^5$ s are comparable to those of the ISS-PIs synthesized from aromatic diamines [32], indicating that the thermal decomposition temperature of ISS-PIs including ISS-APIs is dominated by the ISSDA skeleton which includes ester groups attached to an alicyclic ISS skeleton. Interestingly, ISS-DDA shows a slightly higher  $T_d^5$  of 410 °C, suggesting that the long alkyl chains do not necessarily deteriorate thermal decomposition stability.

### 3.5. Mechanical properties of ISS-APIs

Fig. 10 shows the temperature dependence of the storage modulus ( $E'$ ), loss modulus ( $E''$ ), and  $\tan \delta$

Table 4. Glass transition temperatures ( $T_g$ ), coefficients of linear thermal expansion in the in-plane direction (CTE), 5 wt% weight loss temperatures ( $T_d^5$ ), and  $\beta$ -/ $\alpha$ -relaxation temperatures ( $T_\beta$  and  $T_\alpha$ ) of ISS-APIs.

| Polyimide | $T_g / ^\circ\text{C}$ |      | CTE<br>/ ppm $\text{K}^{-1}$ | $T_d^5 / ^\circ\text{C}$ | $T_\beta / ^\circ\text{C}$ | $T_\alpha / ^\circ\text{C}$ |
|-----------|------------------------|------|------------------------------|--------------------------|----------------------------|-----------------------------|
|           | DSC                    | TMA  |                              |                          |                            |                             |
| ISS-HMDA  | 152                    | 156  | 64                           | 399                      | 78                         | 171                         |
| ISS-OMDA  | 132                    | 138  | 73                           | 400                      | 69                         | 151                         |
| ISS-DDA   | 47                     | < 50 | –                            | 410                      | –                          | 66                          |

measured by DMA for ISS-APIs. As seen in Fig. 10 (a), the  $E'$ s of ISS-APIs at 30 °C are in the 0.9–1.7 GPa, indicating sufficient mechanical strength. Besides, the  $E'$  observed between room temperature and  $T_g$  was almost constant, indicating that the  $\alpha$ -relaxation was readily activated around  $T_g$ . In a magnified view of Fig. 10 (c), small peaks at around 70 °C, namely  $\beta$ -relaxation, were observed for ISS-HMDA and ISS-OMDA. However, this is not attributable to the characteristic motion of the alkyl chains because the crankshaft motion of  $\text{CH}_2$  groups generally occurs at around –140 °C [27]. These peaks could be attributed to a relaxation of the benzoyl groups at the ISSDA moiety, which is induced by the combination of a bulky ISS and flexible alkyl chains [35,44,45]. Note that the approximately 20 °C higher temperature shift of the  $T_\alpha$  compared to the  $T_g$  obtained from DSC and TMA depends on the difference in measurement frequency.

#### 4. Conclusion

A series of ISS-APIs were synthesized from the isosorbide-derived dianhydrides (ISSDA) and three types of diamines having long alkyl chains. The PI films exhibited very low  $n_{av}$  ( $< 1.566$ ) and  $\Delta n$  ( $< 0.00124$ ) in addition to good film formability, a wide range of solubility in organic solvents, and sufficient optical transparency. These are attributable to the weak intermolecular interactions and isotropic molecular orientation due to the flexible alkyl chains. Similarly, ISS-APIs have smaller values of  $D_k$  and  $D_f$  at 10 and 20 GHz than the wholly or semi-aromatic PIs owing to their small contents of polar (imide and ester) groups ( $Polar\%$ ). The reduced dielectric polarization and the relaxation motion occurring far from 10 and 20 GHz result in the smallest values of  $D_k$  (2.52) and  $D_f$  (0.00327) for ISS-DDA with the highest  $Alkyl\%$  and the lowest  $Polar\%$ . Although the alky chains in the PI main chains cause a significant reduction in  $T_g$  due to the enhanced flexibility, ISS-APIs have sufficient thermal decomposition stability with  $T_d^{5\%}$ s around 400 °C and good mechanical strength with  $E'$ s as high as 1.0 GPa. In particular, ISS-DDA derived from a bio-based dimer diamine exhibited excellent overall optical and dielectric properties, such as extremely low values of  $n_{av}$ ,  $\Delta n$ ,  $D_k$ , and  $D_f$ , while achieving the highest  $C_B = 65\%$ . This study provides a new possibility of semi-aliphatic functional PIs applicable to optoelectronics with an added value of bio-based materials.

#### Acknowledgment

This work was in part financially supported by JSPS KAKENHI Grant Number 21H01995.

#### References

1. D. J. Saxon, A. M. Luke, H. Sajjad, W. B. Tolman, and T. M. Reineke, *Prog. Polym. Sci.*, **101** (2020) 101196.
2. F. Fenouillot, A. Rousseau, G. Colomines, R. Saint-Loup, and J. P. Pascault, *Prog. Polym. Sci.*, **35** (2010) 578.
3. H. Nakajima, P. Dijkstra, and K. Loos, *Polymers (Basel)*, **9** (2017) 1.
4. R. P. Babu, K. O'Connor, and R. Seeram, *Prog. Biomater.*, **2** (2013) 8.
5. I. Bechthold, K. Bretz, S. Kabasci, R. Kopitzky, and A. Springer, *Chem. Eng. Technol.*, **31** (2008) 647.
6. R. Auvergne, S. Caillol, G. David, B. Boutevin, and J. P. Pascault, *Chem. Rev.*, **114** (2014) 1082.
7. C. Dussenne, T. Delaunay, V. Wiatz, H. Wyart, I. Suisse, and M. Sauthier, *Green Chem.*, **19** (2017) 5332.
8. O. Gómez-de-Miranda-Jiménez-de-Aberasturi, A. Centeno-Pedraza, S. Prieto Fernández, R. Rodríguez Alonso, S. Medel, J. María Cuevas, L.G. Monsegue, S. De Wildeman, E. Benedetti, D. Klein, H. Henneken, and J. R. Ochoa-Gómez, *Green Chem. Lett. Rev.*, **14** (2021) 534.
9. H. R. Kricheldorf, *J. Macromol. Sci. Part C Polym. Rev.*, **37** (1997) 599.
10. M. Yokoe, K. Aoi, and M. Okada, *J. Polym. Sci. Part A Polym. Chem.*, **43** (2005) 3909–.
11. G. Rabilloud, *High-Performance Polymers: Polyimides in Electronics*, Editions Technip, 2000.
12. S. Ando, Y. Watanabe, and T. Matsuura, *Jpn. J. Appl. Phys., Part 1 Regul. Pap. Short Notes Rev. Pap.*, **41** (2002) 5254.
13. M. C. Choi, Y. Kim, and C. S. Ha, *Prog. Polym. Sci.*, **33** (2008) 581.
14. H. J. Ni, J. G. Liu, Z. H. Wang, and S. Y. Yang, *J. Ind. Eng. Chem.*, **28** (2015) 16.
15. J. O. Simpson and A. K. St. Clair, *Thin Solid Films*, **308–309** (1997) 480.
16. B. V. V. Kotov, T. A. A. Gordina, V. S. S. Voishchev, O. V. V. Kolninov, and A. N. N. Pravednikov, *Polym. Sci. U.S.S.R.*, **19** (1977) 711.
17. R. A. Dine-Hart and W. W. Wright, *Makromol. Chem.*, **143** (1971) 189.
18. S. Ando, T. Matsuura, and S. Sasaki, *Polym. J.*, **29** (1997) 69.
19. M. Hasegawa and K. Horie, *Prog. Polym. Sci.*, **26** (2001) 259.
20. C. Koning, A. Delmotte, P. Larno, and B. Van

- Mele, *Polymer (Guildf)*, **39** (1998) 3697.
21. A. S. Mathews, I. Kim, and C. S. Ha, *Macromol. Res.*, **15** (2007) 114.
  22. Y. Zhuang, J. G. Seong, and Y. M. Lee, *Prog. Polym. Sci.*, **92** (2019) 35.
  23. J. Wakita, S. Jin, T. J. Shin, M. Ree, and S. Ando, *Macromolecules*, **43** (2010) 1930.
  24. T. Matsumoto, *J. Photopolym. Sci. Technol.*, **14** (2001) 725.
  25. Y. Watanabe, Y. Sakai, Y. Shibasaki, S. Ando, M. Ueda, Y. Oishi, and K. Mori, *Macromolecules*, **35** (2002) 2277–2281.
  26. A. S. Mathews, I. Kim, and C. S. Ha, *J. Appl. Polym. Sci.*, **102** (2006) 3316.
  27. A. E. Eichstadt, T. C. Ward, M. D. Bagwell, I. V. Farr, D. L. Dunson, and J. E. McGrath, *J. Polym. Sci. Part B, Polym. Phys.*, **40** (2002) 1503.
  28. A. Susa, R. K. Bose, A. M. Grande, S. Van Der Zwaag, and S. J. Garcia, *ACS Appl. Mater. Interfaces*, **8** (2016) 34068.
  29. A. Susa, J. Bijleveld, M. Hernandez Santana, and S. J. Garcia, *ACS Sustain. Chem. Eng.*, **6** (2018) 668.
  30. J. Liu, K. Wang, Y. Xie, F. Gao, Q. Zeng, Y. Yuan, R. Liu, and X. Liu, *J. Coat. Technol. Res.*, **14** (2017) 1325.
  31. J. Lee, S. Yoo, D. Kim, Y. H. Kim, S. Park, N. K. Park, Y. So, J. Kim, J. Park, M. J. Ko, and J. C. Won, *Mater. Today Commun.*, **33** (2022) 1.
  32. R. Sawada and S. Ando, *Macromolecules*, **55** (2022) 6787.
  33. R. Sawada and S. Ando, *J. Mater. Chem. C*, **11** (2023) 15053–15064.
  34. Y. Terui and S. Ando, *J. Polym. Sci. Part B Polym. Phys.*, **42** (2004) 2354.
  35. T. Okada, R. Ishige, and S. Ando, *Polymer (Guildf)*, **146** (2018) 386.
  36. S. Krimm, C. Y. Liang, and G. B. B. M. Sutherland, *J. Chem. Phys.*, **25** (1956) 549.
  37. L. Lorenz, *Ann. Phys.*, **247** (1880) 70.
  38. G. Maier, *Prog. Polym. Sci.*, **26** (2001) 3.
  39. Y. Ji, Y. Bai, X. Liu, and K. Jia, *Adv. Ind. Eng. Polym. Res.*, **3** (2020) 160.
  40. Z. Zhou, W. Li, J. Qian, W. Liu, Y. Wang, X. Zhang, Q. Guo, Y. Yashchyshyn, Q. Wang, Y. Shi, and Y. Zhang, *Molecules*, **27** (2022) 1336.
  41. G. Hougham, G. Tesoro, A. Viehbeck, and J. D. Chapple-Sokol, *Macromolecules*, **27** (1994) 5964.
  42. Y. Oishi, W. Miura, H. Hirahara, and K. Mori, *J. Photopolym. Sci. Technol.*, **12** (1999) 217.
  43. B. K. Chen, T. Y. Wu, C. H. Lin, and J. M. Wong, *Fibers Polym.*, **14** (2013) 1051.
  44. X. Ji, J. Yan, X. Liu, Z. Wang, and Z. Wang, *High Perform. Polym.*, **29** (2017) 197.
  45. X. Ji, Z. Wang, Z. Wang, and J. Yan, *Polymers (Basel)*, **9** (2017) 569.